Drug Design, Development and Therapy

Dovepress
Taylor & Francis Group

Open Access Full Text Article

ORIGINAL RESEARCH

Hepatoprotective Effects of Fused Pyridine Derivatives: Regulation of the TGF-β/Smad, miR-21/Smad7, and PPARγ Pathways in Carbon Tetrachloride-Induced Liver Fibrosis

Mahmoud Mohamed Khalil[1], Reem H Elhamammy[1], Hanan M Ragab[2], Mohamed Hussein Abdelgalil[1], Eman Sheta[3], Ahmed R Elaraby[4], Tamer M Ibrahim[5,6], Ahmed Wahid[1]

[1]Department of Biochemistry, Faculty of Pharmacy, Alexandria University, Alexandria, Egypt; [2]Department of Pharmaceutical Chemistry, College of Pharmacy, Al-Farahidi University, Baghdad, 10021, Iraq; [3]Department of Pathology, Faculty of Medicine, Alexandria University, Alexandria, Egypt; [4]Department of Pharmaceutical Chemistry, Faculty of Pharmacy, Sinai University, Kantara Branch, Ismailia, Egypt; [5]Department of Pharmaceutical Chemistry, Faculty of Pharmacy, Kafrelsheikh University, Kafrelsheikh, Egypt; [6]Department of Pharmaceutical Chemistry, Faculty of Pharmacy, The British University in Egypt, Al-Sherouk City, Cairo, Egypt

Correspondence: Ahmed Wahid, Department of Biochemistry, Faculty of Pharmacy, Alexandria University, Alexandria, Egypt, Tel +201125566987, Email ahmed.wahid@alexu.edu.eg

Background: The liver functions as the body's central metabolic organ, responsible for a wide array of vital processes, making its protection a key objective in medical research. Consequently, the promising hepatoprotective potential of several 4-phenyltetrahydroquinoline derivatives motivated us to comprehensively investigate the mechanisms of action of four newly synthesized compounds on carbon tetrachloride (CCl_4)-induced liver injury in rats.

Methods: Liver tissues and serum samples were collected from all experimental groups of Sprague-Dawley rats for histopathological examination, serological testing, RT-PCR, and ELISA. The mRNA expression levels of TGF-β, Smad2, α-SMA, Col1a1, Smad7, miR-21, and PPARγ, along with the protein levels of MMP-9 and TGF-β, were analyzed in liver tissues. Additionally, the HepG2 cell line was used for in vitro hepatotoxicity testing.

Results: The mRNA expression of miR-21, Smad2, α-SMA, Col1A1, and TGF-β, as well as the protein levels of TGF-β and MMP-9, was reduced in rats treated with our compounds compared to CCl_4-induced liver fibrosis in adult male Sprague-Dawley rats. Conversely, these compounds increased the mRNA expression of Smad7 and PPARγ. Additionally, the histopathological analysis showed a decrease in the degree of liver fibrosis following treatment with the tested compounds.

Conclusion: The tested fused pyridine derivatives may protect the liver from fibrosis by modulating the TGF-β/Smad, miR-21-regulated TGF-β/Smad7, and PPARγ signaling pathways. These findings suggest that these derivatives could serve as novel agents for protecting the liver against fibrosis.

Keywords: liver fibrosis, 4-phenyltetrahydroquinoline derivatives, rats, hepatotoxicity, CCl_4, TGF-β, Smad, PPARγ, miR-21

Introduction

Liver fibrosis is a reversible pathophysiological process, serving as a compensatory reaction and wound-healing response triggered by various pathological factors. Persistent hepatic damage resulting from inherited or acquired factors, including metabolic disorders, viral infections, alcohol abuse, autoimmune diseases, and exposure to hepatotoxic agents,[1] can compromise the liver's regenerative capacity and lead to progressive pathological changes ranging from transient elevations in liver enzymes to hepatic fibrosis, cirrhosis, and ultimately hepatocellular carcinoma.[2,3] The global incidence and prevalence of liver fibrosis have been on the rise in recent years in global population as reported by Zamani et al in 2025,[4] posing a significant worldwide health challenge.[5] Hepatic stellate cells (HSCs) are specialized cells located throughout the liver, and they play a vital role in both normal liver function and in responses to injury. These cells

https://doi.org/10.2147/DDDT.S592956
Received: 31 December 2025
Accepted: 24 March 2026
Published: 8 April 2026

become activated in the presence of liver damage, stimulated by various cytokines such as transforming growth factor beta (TGF-β). The activation of HSCs is a crucial factor in the initiation and progression of liver fibrosis.[5,6] Although HSCs are typically quiescent, once activated, they undergo behavioral alterations, becoming proliferative and fibrogenic. This transformation leads them to differentiate into myofibroblasts, culminating in the buildup of extracellular matrix (ECM).[7] Interestingly, research suggests a down-regulation of hepatic stellate cells in normal liver tissue.[8]

Transforming growth factor-β (TGF-β) serves as a crucial activator of hepatic stellate cells (HSCs) and exerts regulatory control over various biological processes, encompassing the cell growth cycle, cell differentiation, immune modulation, and deposition of extracellular matrix.[9] The TGF-β pathways play a significant role in the development of liver fibrosis.[8] There are two distinct TGF-β signaling pathways governing fibrosis: the canonical pathway, involving SMAD-2/3, and the non-canonical pathway, which operates independently of SMAD-2/3 participation.[9] In the canonical TGF-β signaling pathway, the initial step involves the release of active TGF-β from the latent TGF-β complex situated in the extracellular space, where it exists in an inactive state. Following this, the inactive TGF-β molecule binds to the TGF-β type II receptor (TGF-βRII), initiating the phosphorylation of the TGF-β type I receptor ALK5. This activation sets off a cascade of events, leading to the continuous phosphorylation of Smad2 and Smad3 proteins by ALK5 in the cytoplasm. Subsequently, these phosphorylated proteins form a complex with Smad4, which translocate to the nucleus. In the nucleus, this complex regulates fibrosis-related transcription by interacting with various transcription factors, thereby influencing gene transcription of molecules like type I collagen (Col1a1), α-smooth muscle actin (α-SMA), Matrix metalloproteinases (MMPs), and tissue inhibitors of metalloproteinases (TIMPs) in HSCs.[8,9] Additionally, the inhibitory function of SMAD-7 competes with SMAD-2/3 to bind to phosphorylated ALK5.[8,9] Concurrently, various studies have affirmed that inhibiting TGF-β expression and modulating the TGF-β/Smad signaling pathway are effective strategies for preventing liver fibrosis.[10]

Matrix metalloproteinases, a diverse family of endopeptidases capable of degrading nearly all ECM components. They are typically secreted as inactive proenzymes with tightly regulated activity, the dysregulation of which can lead to tissue damage and functional alterations, and their proteolytic activities in tissues are controlled by TIMPs.[11]

Peroxisome proliferator-activated receptor-γ (PPAR-γ) has a pivotal role in the activation and phenotypic alteration of HSCs. PPAR-γ helps keep HSCs in a quiescent state, suppressing the production of col1a1, α-SMA, and TGF-β, thereby playing a vital role in reducing and preventing liver fibrosis. The effects of PPAR-γ involve disrupting the TGF-β signaling pathway and Smad-dependent promoter activity. It directly opposes the activation and/or function of Smad3 in fibroblasts, without affecting the protein expression of stimulatory Smad3. Additionally, PPAR-γ enhances the expression of inhibitory Smad7.[12]

MicroRNAs (miRNAs) are a class of small RNAs that are endogenous and non-coding single-stranded RNAs. They function by binding to target genes, resulting in the suppression of target gene translation and/or the degradation of target gene mRNA. The dysregulation of miRNAs has been implicated in the pathogenesis of various diseases, including fibrotic conditions.[9]

Notably, miRNA-21 emerges as a key player, exerting multifunctional control over several signaling pathways, including TGF-β/Smads. Specifically, miR-21 can augment the activity of the TGF-β/SMAD-2/3 signaling pathway by suppressing the expression of Smad7. This, in turn, contributes to the promotion of the fibrotic process in the liver.[9] Consequently, targeting miR-21 expression and thereby inhibiting the TGF-β1/Smad2-3 signaling pathway may alleviate hepatic fibrosis, suggesting that miR-21 holds promise as a therapeutic target for treating hepatic fibrosis.[13]

Carbon tetrachloride (CCl_4) is a common toxic chemical known for its ability to cause immediate liver damage. Carbon tetrachloride-induced hepatic injury is a well- established model for the study of liver fibrogenesis. Following metabolic activation by cytochrome P450 enzymes, particularly CYP2E1, CCl_4 is converted into highly reactive trichloromethyl ($\bullet CCl_3$) and trichloromethyl peroxyl ($\bullet OOCCl_3$) radicals, which initiate lipid peroxidation, oxidative stress, and hepatocellular membrane damage.[14] This oxidative injury results in hepatocyte necrosis, inflammatory cell infiltration, and the release of profibrotic mediators that subsequently trigger hepatic stellate cell activation.[15] Repeated administration of CCl_4 leads to sustained hepatocellular injury, excessive ECM deposition, and progressive fibrosis, closely mimicking key pathological features of human liver fibrogenesis.[16] Histologically, livers of CCl_4-treated animals

exhibit marked morphological alterations including fatty degeneration, hepatocyte ballooning, centrilobular necrosis, inflammatory infiltration, and collagen accumulation compared with control animals.[17]

Fused pyridine (Tetrahydroquinoline "THQ") derivatives hold significant importance in medicinal chemistry due to their wide range of pharmacological activities.[18–22] Notably, these derivatives have been recognized for their hepatoprotective properties.[23] Several derivatives were synthesised in our laboratories, which have shown efficacy in reducing elevated ALT levels in rats.[18,24] These compounds were designed based on the structure of the acetylcholinesterase inhibitor (tacrine).[25] Literature reviews consistently highlight the role of tetrahydroquinoline derivatives as hepatoprotective agents, particularly emphasizing the importance of substituents at the 2- and 4-positions of the tetrahydroquinoline nucleus.[14,26,27]

Our aim in this study is to evaluate the hepatoprotective effects of four novel fused pyridine derivatives, assess their safety profile in hepatocytes, and elucidate the potential mechanisms and pathways underlying their actions. The introduced groups at positions 2-, 3- and 4- of the tetrahydroquinoline nucleus were chosen carefully to investigate the electronic and steric effects of substituents at these positions.

Materials and Methods

Chemicals and Drugs

Dimethyl sulfoxide (DMSO) was purchased from Thermo-Fisher Scientific (USA). Dulbecco's Modified Eagle Medium (DMEM) and fetal bovine serum (FBS) were obtained from Biowest (France). Tacrine was sourced from Sigma-Aldrich Co. (St. Louis, MO, USA). Corn oil and CCl_4 were acquired from Alpha Chemika (India). Carboxymethyl cellulose sodium salt (CMC) and formalin were purchased from Adwic - El Nasr Pharmaceutical Co. (Egypt). Silymarin and isoflurane 100% were procured from Pharco-Pharmaceuticals Inc. (Egypt). Phosphate-buffered saline was obtained from Loba Chemie (Mumbai, India).

Compound Synthesis

Compounds shown in Figure 1 have been synthesized according to procedure reported by Ragab et al.[18] Further details are available at supplementary materials (SM).

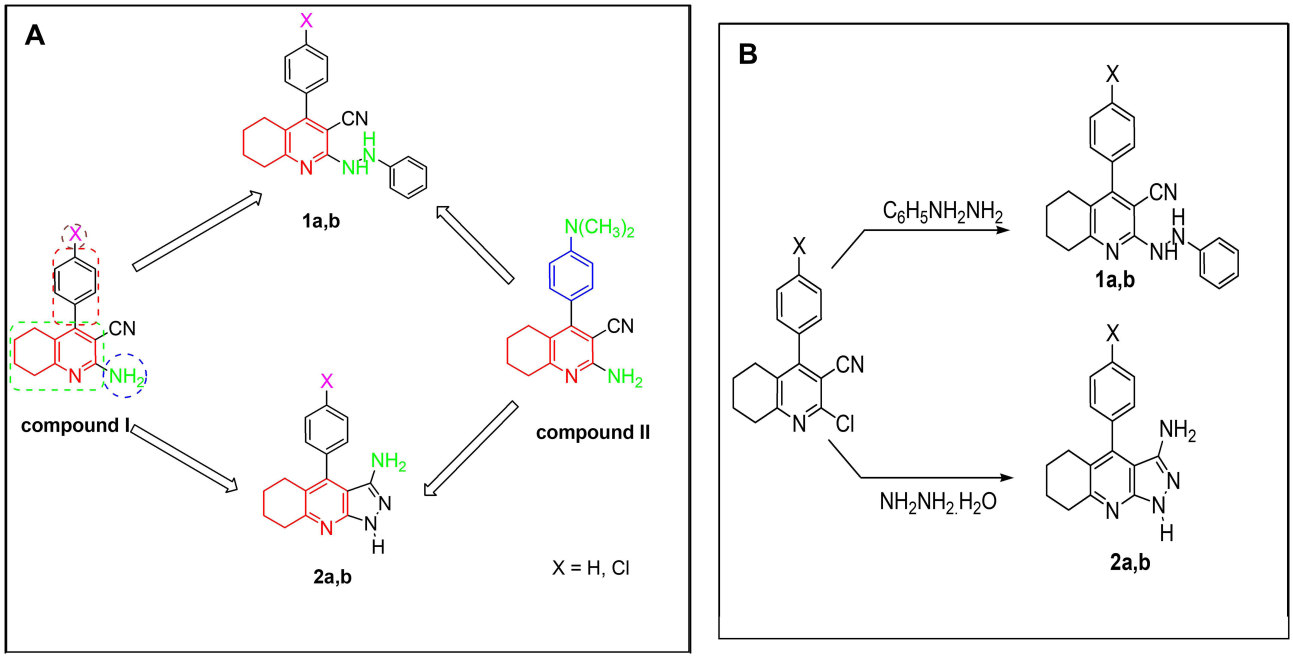

Figure 1 (**A**) Rational for the synthesis of compounds 1a, 1b, 2a, and 2b. (**B**) Scheme for synthesis of target compounds. For compounds 1a, b: synthesis involves the substitution of 2-chlorotetrahydroquinolines with 2 equivalents of phenyl hydrazine. For compounds 2a, b: synthesis involves the substitution of 2-chlorotetrahydroquinolines with 2 equivalents of hydrazine hydrate (98%).

https://doi.org/10.2147/DDDT.S592956

2-(2-Phenylhydrazinyl)-4-phenyl-5,6,7,8-tetrahydroquinoline-3-carbonitrile (1a)[18]
Yield 65%; m.p.: 134–136 °C
4-(4-Chlorophenyl)-2-(2-phenylhydrazinyl)-5,6,7,8-tetrahydroquinoline-3-carbonitrile (1b)[18]
Yield 60%; m.p.: 179–181 °C
3-Amino-4-phenyl-5,6,7,8-tetrahydro-1H-pyrazolo[3,4-b]- quinoline (2a)[18]
Yield 96%; m.p.: 264–266 °C
3-Amino-4-(4-chlorophenyl)-5,6,7,8-tetrahydro-1H-pyrazolo[3,4-b]quinolone (2b)[18]
Yield 94.5%; m.p.: 254 °C

Biochemical and Molecular Investigations

Cell Culture and MTT Assay

Human hepatoma (HepG2) cells were used to evaluate the in vitro cytotoxicity of the tested compounds compared to tacrine as their structure is derived from it. The HepG2 cell line was obtained from ATCC. The cells were cultured in DMEM with high glucose, supplemented with 10% FBS, 100 U/mL penicillin, and 1% streptomycin were maintained in a 37°C incubator with 5% CO_2 in a humidified atmosphere. One day before the treatment, cells were seeded at a density of 1×10^4 cells/well in a sterile fat bottom 96-well tissue culture plate. After leaving the cells to adhere for 24 h, cells were treated with different concentrations (two-fold serial dilutions ranging from 400 to 25 μM) of each compound as well as tacrine for 24 h in the 5% CO_2 incubator. Thereafter, cell viability was assessed using a 3-(4,5-dimethyl-2-thiazolyl)-2,5-diphenyl-tetrazolium bromide (MTT) assay obtained from Biobasic Inc (Canada).[28] Following the 24-h treatment period, MTT was added to the wells at a final concentration of 0.5 mg/mL, and the cells were incubated for 4 h in the dark. Subsequently, the media were carefully removed from the wells, and the formed formazan crystals were dissolved by adding 100μL of DMSO. Absorbance readings were taken using a microplate reader (BioTek, USA), and the percentage cell viability was calculated for each condition relative to the control cells treated with the same DMSO concentration.

Animal Studies

Ninety six (96) Sprague-Dawley male rats weighing 180–220g are included in the study and were obtained from the animal house at the Institute of Graduate Studies and Research, Alexandria University, Egypt. Rats were kept at room temperature, under a 12-h light/dark cycle, in well-ventilated polypropylene cages, and had free access to water and food. This study was conducted in accordance with the ARRIVE Guidelines and the Guide for the Care and Use of Laboratory Animals to ensure the welfare of laboratory animals and was approved (Approval Code: 06-2023-4–12-2-178) by the Animal Care and Use Committee of the Faculty of Pharmacy, Alexandria University.

Experimental Design

Rats were randomly divided into twelve groups (n = 8). Group I, the healthy rats, do not receive any drug or diluent. Group II, the control group, received corn oil (1 mL/kg body weight, i.p.) every 72 h for 14 days. Group III, the hepatotoxicity group, received CCl_4 (1 mL/kg body weight, a 1:1 v/v mixture of CCl_4 and corn oil, i.p.) every 72 h for 14 days.[29] Groups IV–VII, the treated groups, received compounds (1a, 1b, 2a, and 2b), respectively, (25 mg/kg body weight, suspended in 0.5% CMC, P.O.) every 24 h, as well as CCl_4 (1 mL/kg body weight, a 1:1 v/v mixture of CCl_4 and corn oil, i.p.) every 72 h for 14 days. Group VIII, the positive control group, received silymarin (100 mg/kg, suspended in 0.5% CMC, P.O.) every 24 h, as well as CCl_4 (1mL/kg body weight, a 1:1 v/v mixture of CCl_4 and corn oil, i.p.) every 72 h for 14 days.[30] Groups IX–XII, the safety profile groups, received only compounds (1a, 1b, 2a, and 2b), respectively, (25 mg/kg, suspended in 0.5% CMC, P.O.) every 24 h for 14 days. The dose of the newly synthesized compounds (25 mg/kg/day, orally) was selected based on the therapeutic dose of tacrine, which had been shown to maintain cholinergic-mediated behaviors in rats in a prior study examining the pharmacokinetic and pharmacodynamic properties of tacrine and other cholinesterase inhibitors.[31] Additionally, in two prior studies from our laboratory using two other sets of four tacrine-derived compounds each, the same dose demonstrated full safety in comprehensive assessments and effective hepatoprotection.[14,27]

Sample Collection and Preparation

Rats were euthanized 24 hours after the final treatment dose using an inhaled overdose of isoflurane.[32] Blood was collected via cardiac puncture, allowed to coagulate, and then centrifuged for 10 minutes at 5000 rpm (GBF501, Centrifuge Cencom-II, Selecta) to obtain serum. The livers were collected and dissected into portions. One portion was fixed overnight in 10% buffered formalin for histological examination. Another portion was homogenized and centrifuged at 10,000 rpm for 10 minutes, with the supernatants collected for further analysis. Liver tissues and homogenates were stored at −80°C until used.

Biochemical Analysis

Various colorimetric serum diagnostic kits were used to evaluate the toxicity and hepatoprotective potential of the newly synthesized derivatives. To assess the toxicity profile, lipid parameters such as total cholesterol (TC) and triglycerides (TG) were measured. For the assessment of hepatotoxicity and hepatoprotective potential, liver function tests including ALT (alanine transaminase), AST (aspartate transaminase), alkaline phosphatase (ALP), and total bilirubin (TBIL) were conducted. All diagnostic kits were obtained from Biodiagnostics, Egypt, and were used and stored according to the manufacturer's instructions.

Histopathological Assessment

Serial sections were prepared from the formalin-fixed liver tissues, which were then processed into paraffin blocks. Multiple 5-µm-thick sections were cut and mounted on glass slides. One section was stained with H&E to assess activity, while another was stained with Masson trichrome to evaluate fibrosis. Both activity and fibrosis were examined using a light microscope (Olympus, CX 22LED) and assessed with the METAVIR scoring system.[33] For activity, the number of inflammatory foci (lobular necrosis) and the degree of portal inflammation (piece meal necrosis) were evaluated, resulting in a histological activity score (A0 = none, A1 = mild, A2 = moderate, A3 = severe). Fibrosis was assessed on Masson trichrome-stained sections and scored according to a 4-tiered system (F0 = no fibrosis, F1 = mild/moderate, F2 = significant, F3 = advanced fibrosis, F4 = cirrhosis). Moreover, at x200 power, Masson trichrome stained photos were assessed by image analysis software. The blue colour of fibrous tissue was extracted and measured as percentage of total image area. Additionally pathological features, such as steatosis and apoptotic hepatocytes, were also noted if present.

Enzyme-Linked ImmunoSorbent Assay (ELISA)

Expression of both TGF-β and MMP-9 in liver tissues was determined by sandwich ELISA using ELISA kits (Catalog Numbers: BYEK3197, Chongqing Biospes Co., Ltd., China, and Catalog Numbers: E-EL-R3021, Elabscience, USA, respectively).

Quantitative Real-time Polymerase Chain Reaction

Quantitative analysis of studied genes (TGFβ, Smad2, α-SMA, Col1a1, Smad7 and PPARγ), and miR-21 expression in liver tissues were performed using quantitative real time reverse transcriptase-polymerase chain reaction (qRT-PCR). Concerning (TGFβ, Smad2, α-SMA, Col1a1, Smad7 and PPARγ) first, the total RNA was isolated from the liver tissues using the phenol/guanidine extraction method (miRNeasy Mini Kit, catalog number: 217004, QIAGEN, Germany), according to the manufacturer instructions, then the isolated RNA was reverse transcribed using (QuantiTect Reverse Transcription Kit, Catalog no. 205311, QIAGEN, Germany) into complementary DNA (cDNA). Quantitative PCR was applied to determine the relative expression of studied genes using the (ViPrime PLUS Taq qPCR Green Master Mix I Kit, Catalog no. QLMM12-LR, Viviantis, Malaysia) and the specific primer sets for each gene (Table 1). The relative quantification (RQ) using comparative threshold cycle (Ct) provides an accurate comparison between the initial levels of template in each sample. A normalizer or reference gene (18s rRNA) was used as internal control for experimental variability in this type of quantification. This method of relative quantification is called 2-ΔΔCt method or Livak method. Quantitative PCR assay was carried out using Bio-Rad CFX connect thermal cycler (Bio-Rad, Inc USA).[34]

Concerning miR-21 expression in the hepatic tissue was assayed using TaqMan® miR-21 (Thermo Fisher Scientific, Cat.no. 4427975, ID: 000397) kit and using U6 as a reference gene (cat no. 4427975, ID: 001973). Quantitative PCR

Table 1 Primer Sets of Studied Genes and 18s rRNA (Reference Gene)

Gene	Accession No.	Primer Sequence	
ASMA	NM_001106409.1	**Forward**	TGCTGACAGAGGCACCACTGAA
		Reverse	CAGTTGTACGTCCAGAGGCATAG
COL1A1	NM_053304.1	**Forward**	ATCAGCCCAAACCCCAAGGAGA
		Reverse	CGCAGGAAGGTCAGCTGGATAG
PPARγ	NM_013124.3	**Forward**	TGGAGCCTAAGTTTGAGTTTGC
		Reverse	TGAGGTCTGTCATCTTCTGGAG
SMAD2	NM_001277450.1	**Forward**	CCAGGTCTCTTGATGGTCGT
		Reverse	GGCGGCAGTTCTGTTAGAAT
SMAD7	NM_030858.2	**Forward**	GTCCAGATGCTGTACCTTCCTC
		Reverse	GCGAGTCTTCTCCTCCCAGTAT
TGF-1β	NM_021578.2	**Forward**	TGATACGCCTGAGTGGCTGTCT
		Reverse	CACAAGAGCAGTGAGCGCTGAA
18s rRNA (Reference gene)	NR_046237.2	**Forward**	GTAACCCGTTGAACCCCATT
		Reverse	CAAGCTTATGACCCGCACTT

began with an initial denaturation at 95°C for 10 minutes and amplification via 45 cycles of PCR as follows: Denaturation at 95°C for 5 seconds, annealing at 55°C for 15 seconds, and then extension at 60°C for 15 seconds. Amplification, data acquisition, and analysis were performed on CFX96 Touch Deep Well Real-Time PCR Detection System (Bio-rad laboratories, California, USA). The values of threshold cycle (Ct) were determined by CFX Maestro™ Software version 1.1 (Bio-rad laboratories, California, USA). The relative change in miR-21 in samples was determined using the 2-ΔΔCt method and normalized to the reference U6.

Statistical Analysis

GraphPad Prism software (version 10) was used for statistical analysis. For parametric data, results were presented as means ± SEM, and the differences between groups were analyzed using one-way ANOVA followed by Dunnett's post-hoc test. Histopathological nonparametric data were analyzed using the Kruskal–Wallis test, followed by Dunn's multiple comparisons test, and presented as medians (minimum to maximum). A p-value <0.05 was considered statistically significant.

Molecular Modeling and Simulation

The docking experiments and molecular dynamics simulations methodology are detailed in the SM.The molecular dynamics simulations were performed using the StreaMD automated pipeline,[35] employing GROMACS 2023.4.[36] Depictions of the docking poses were constructed using Flare.[37]

Results

In vitro Cytotoxicity Assay

The MTT assay showed that increasing the concentration of the four tested compounds (1a, 1b, 2a, and 2b) did not significantly affect cell viability, while tacrine decreased cell viability with increase in concentration as shown in Figure 2.

In vivo Toxicity Studies

The oral administration of the tested compounds only, groups (IX–XII), showed no significant elevation in alanine transaminase (ALT) compared to both control and health group Figure 3A). One of the tested compounds (1b) also show no significant change to the aspartate transaminase (AST) compared to both control and health group while the other three tested compounds (1a, 2a and 2b) show a significant decrease in AST compared to the control group (Figure 3B). The tested compounds also demonstrated no significant increase in lipid profile (either total cholesterol or triglyceride levels) compared to the control group (Figure 3C and D).

Histopathological assessment of the safety of tested compounds on liver tissues of rats shows preserved architecture and normal histology in H&E stained sections and Masson's trichrome stain shows no fibrosis (Figure 3E).

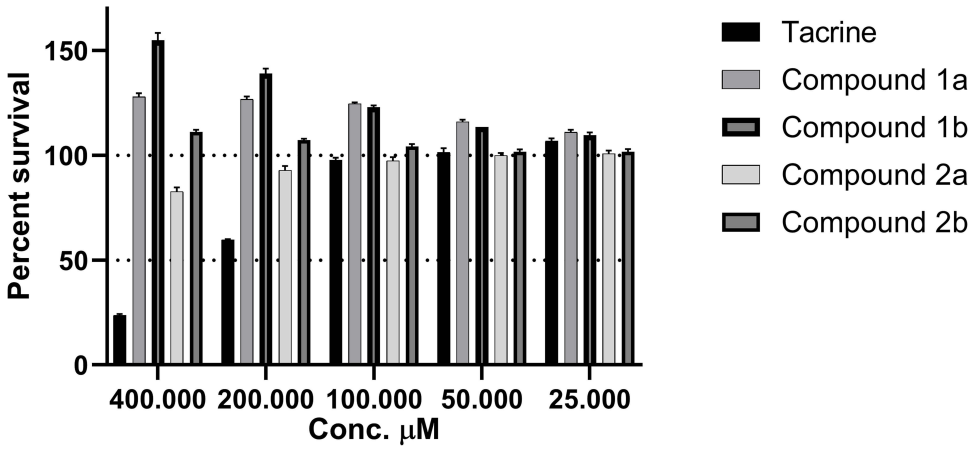

Figure 2 The effect of tested Compounds (1a, 1b, 2a, and 2b) and tacrine on survival of HepG2 cells.

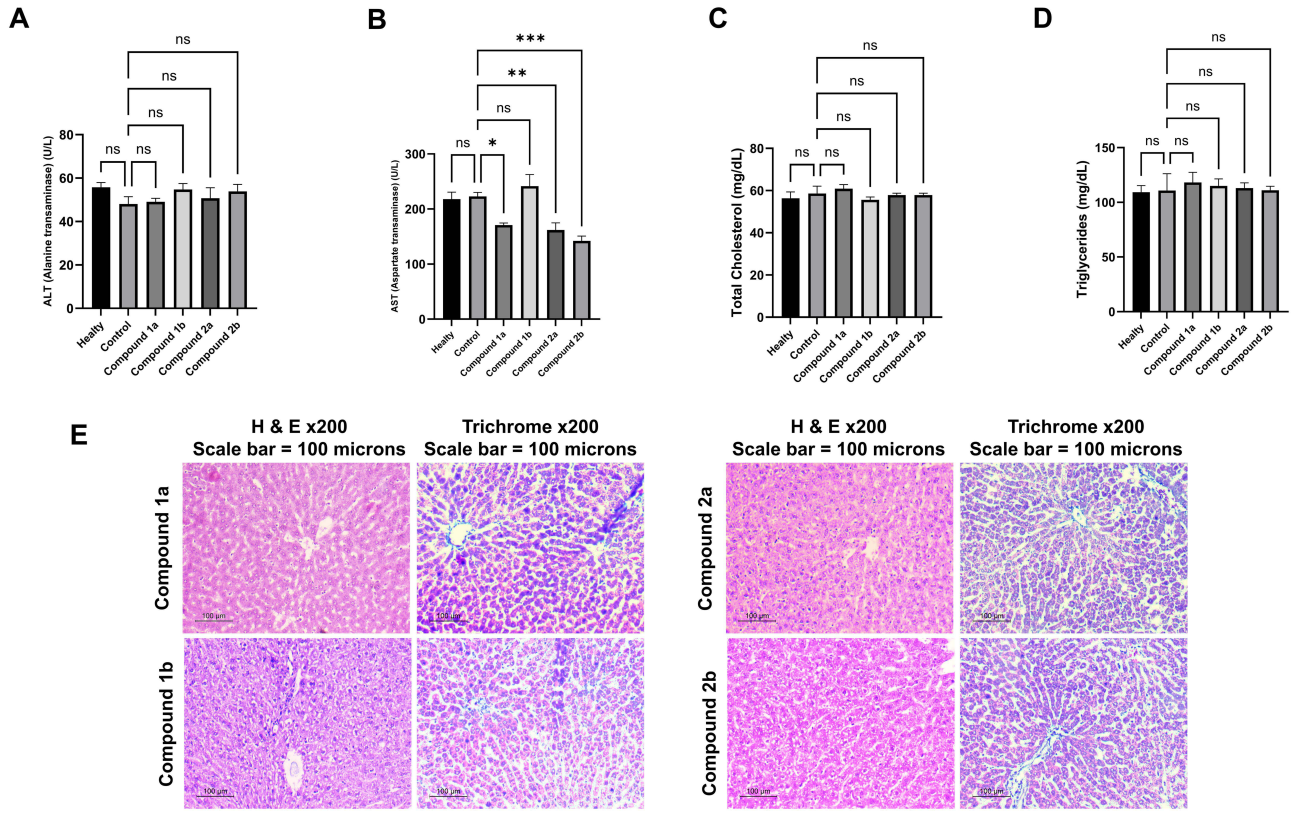

Figure 3 The safety profile of tested compounds (**A**) ALT (alanine transaminase). (**B**) AST (aspartate aminotransferase). (**C**) Total cholesterol. (**D**) Triglycerides. (**E**) Histopathological assessment of liver tissues showing preserved hepatic architecture and normal histology in H&E stained sections (H&E ×200, scale bar = 100μm), while Masson's trichrome stain (×200, scale bar = 100 μm) shows no evidence of fibrosis. Data are presented as mean ± SEM. *p < 0.05, **p < 0.01, ***p < 0.001 compared with the control group.

In vivo Hepatoprotective Activity

Serological Effect of Tested Compounds

In the groups treated with the tested compounds under investigation along with CCl_4 (groups IV–VII) and also the reference drug "silymarin" (group VIII), a significant reduction in ALT, AST, ALP, and total bilirubin levels was observed when compared with the hepatotoxicity group (group III) (Figure 4).

https://doi.org/10.2147/DDDT.S592956

Histopathological Effect of Tested Compounds

Histological examination of liver tissues was conducted to further validate the aforementioned results using both hematoxylin and eosin (H&E) (Figure 5) and Masson's trichrome stains (Figure 6) for accurate assessment of hepatic cell morphology, tissue architecture, and fibrotic changes. Histologic activity grade in different studied groups in H&E stained liver sections was employed. Normal hepatic histology is seen in control groups. Piece meal necrosis is seen in hepatotoxicity group where portal tracts are infiltrated by lymphocytes and plasma cells that extend to nearby peri portal hepatocytes. A focus of lobular necrosis is also seen. Piece meal necrosis was still seen in the tested compounds (1a and 1b). It was improved in the tested compound (2a) which shows only mild inflammation in portal tract. Meanwhile, much improvement was seen in the tested compound (2b) and silymarin groups where minimal or no activity is seen.

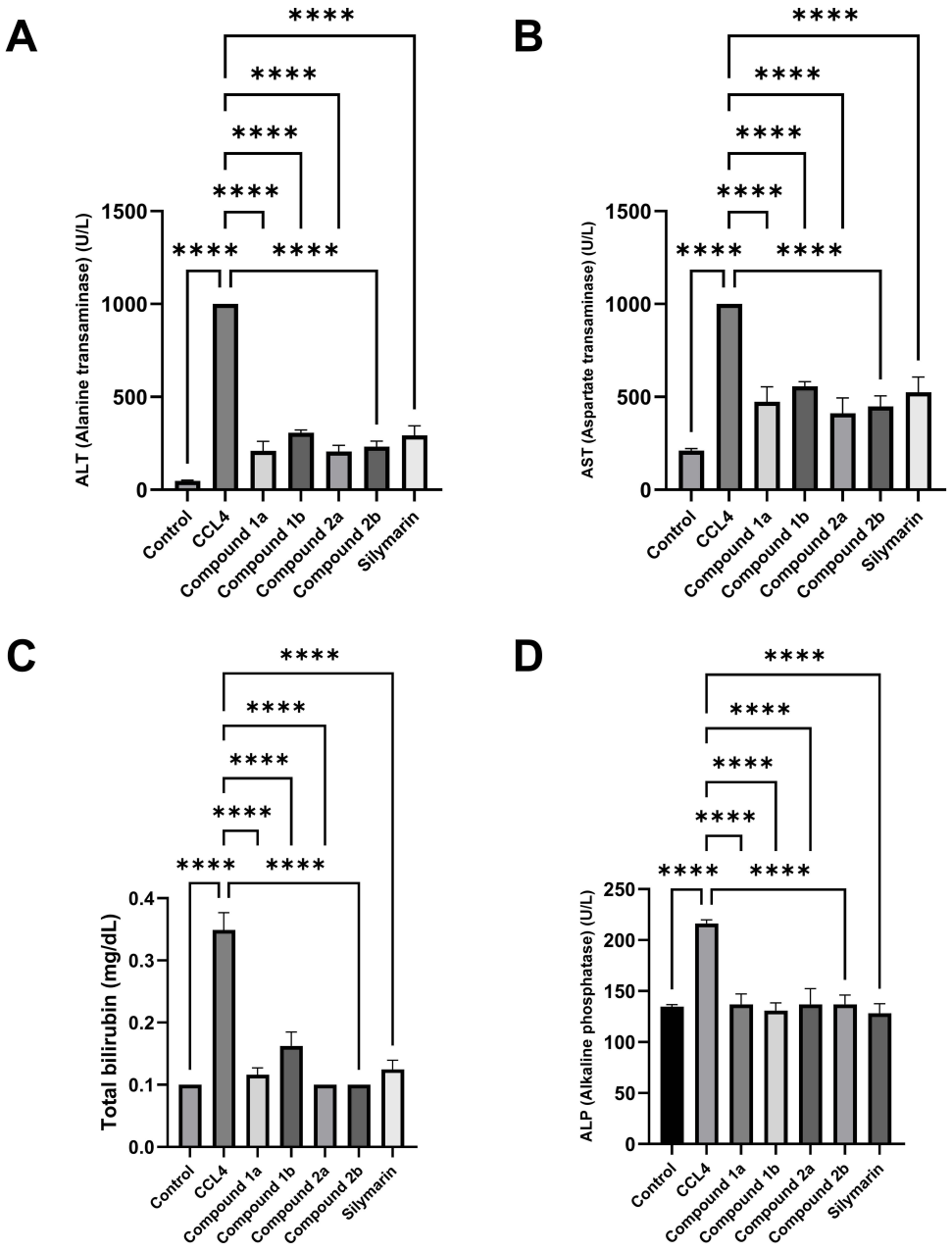

Figure 4 The effect of tested compounds on serum liver biomarkers. (**A**) Alanine transaminase. (**B**) Aspartate transaminase. (**C**) Alkaline phosphatase. (**D**) Total bilirubin. Values are represented as the mean ± SEM, ****p < 0.0001 compared to the hepatotoxicity group.

https://doi.org/10.2147/DDDT.S592956

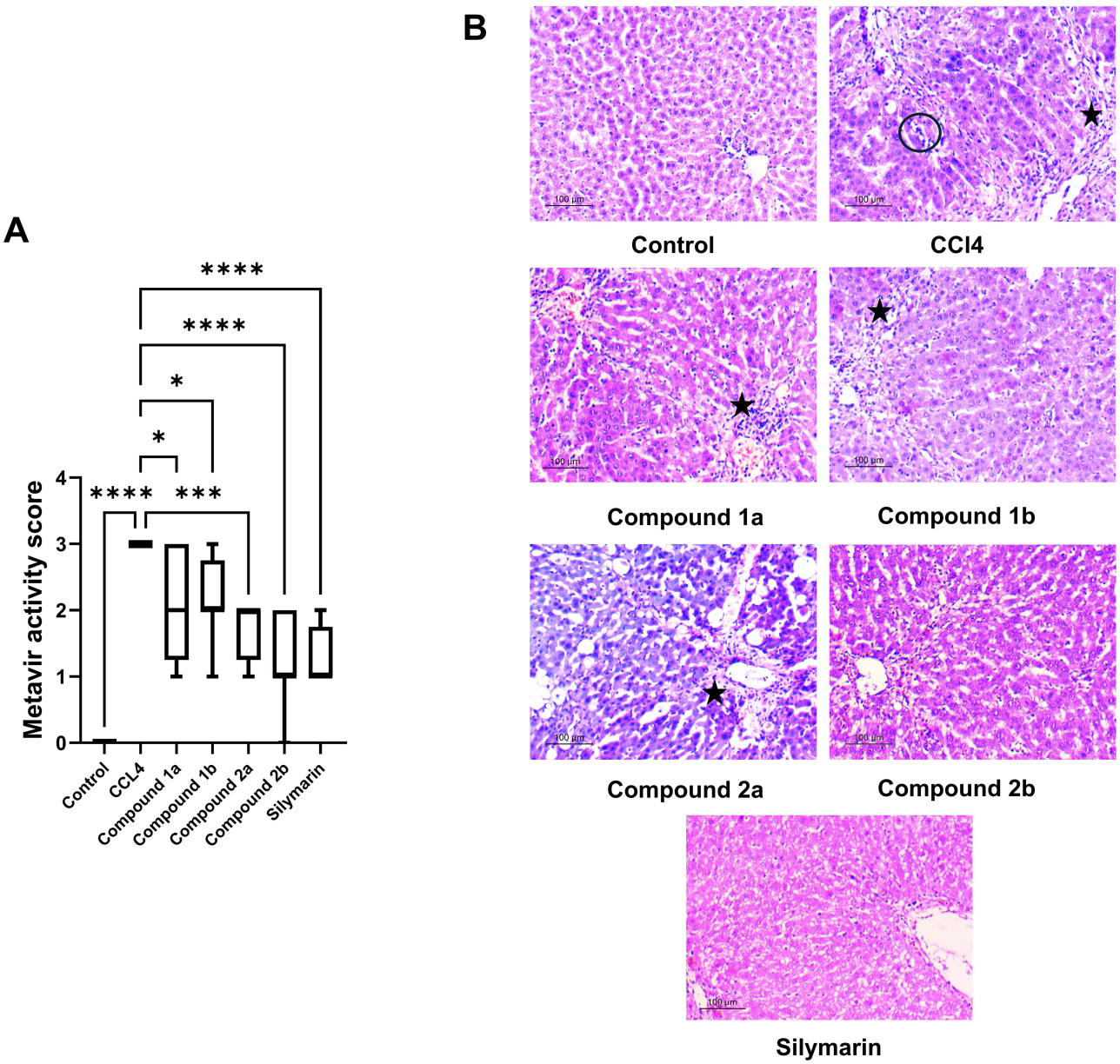

Figure 5 The effect of tested compounds on hepatic histological activity. (**A**) Histological activity grades in liver tissues expressed according to the METAVIR scoring system. Data are presented as median (minimum to maximum) using box-and-whisker plots. *p < 0.05, ***p < 0.001, ****p < 0.0001 compared with the hepatotoxicity group. (**B**) Representative H&E stained liver sections (×200, Scale bar = 100 µm) showing histologic activity in the different studied groups. The hepatotoxicity group shows piecemeal necrosis (star) seen in the form of portal inflammation extending to nearby hepatocytes and lobular necrosis (black circle). Compounds 1a and 1b show moderate piecemeal necrosis (star), whereas compound 2a shows only mild inflammation in the portal tract (star).

Fibrosis stage in Masson's trichrome liver stained sections in different studied groups. In control groups, portal tracts are small and surrounded by minimal fibrous tissue (F0). In hepatotoxicity group, liver is nodular and bridging fibrous bands are seen connecting portal tracts with evident nodular architecture (F4). In the tested compounds (1a and 1b), slight improvement of hepatic histology is seen where portal tracts are expanded with bridging, however, infrequent nodules are present. In the tested compound (2a), portal tracts are expanded with long fibrous septea but bridging is occasional. Much improvement is seen in the tested compound (2b) and sylimarin rats where portal tracts are small or only slightly expanded and short radiating septea are uncommonly seen. Moreover, semi-quantitative analysis of Masson's trichrome-stained sections demonstrated a significant increase in collagen deposition in the CCl_4-treated group compared with the normal control group. Treatment with the tested

https://doi.org/10.2147/DDDT.S592956

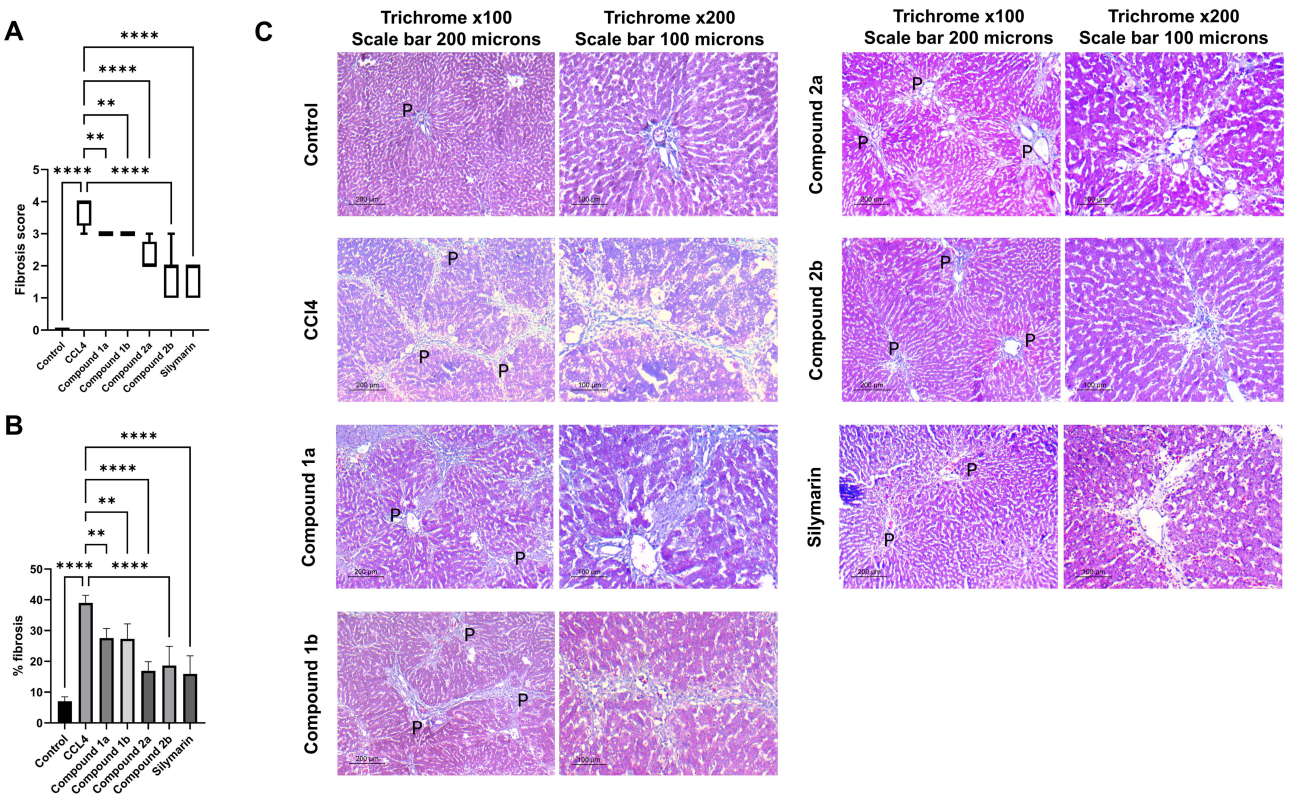

Figure 6 The effect of tested compounds on hepatic fibrosis. (**A**) Fibrosis stages in liver tissues expressed according to the METAVIR scoring system. Data are presented as median (minimum to maximum) using box-and-whisker plots. **p < 0.01, ****p < 0.0001 compared with the hepatotoxicity group. (**B**) Semi-quantitative analysis of fibrosis expressed as fibrotic area (%), calculated as the percentage of collagen-positive area relative to the total tissue area (**C**) Representative liver sections stained with Masson's trichrome stain showing fibrosis in the different studied groups. Low magnification (×100, scale bar = 200μm) highlights the overall liver architecture, while higher magnification (×200, scale bar = 100μm) focus on a representative portal tract. In control group, portal tract (p) is small and rimmed by thin blue fibrous tissue. In CCL4 group, portal tracts (p) are expanded with long fibrous septea is extending from portal tract to another (bridging) forming a nodular liver cut section. Different degrees of restoration of liver architecture is noted in different treatment groups.

fused pyridine derivatives markedly reduced collagen accumulation, as indicated by a significant decrease in the collagen area percentage compared with the CCl_4 group.

Monitoring the Effects of the Tested Compounds on the TGF-β/Smad Pathway

Effect of Tested Compounds on Gene Expression of TGF-β

As shown in Figure 7A, compared with the control group, the mRNA levels of TGF-β, in the hepatotoxicity group were significantly increased (P < 0.0001). After treatment with the four tested compound and silymarin, the mRNA levels of TGF-β was significantly decreased, compared with the hepatotoxicity group.

Effect of Tested Compounds on Gene Expression of Smad-2

Quantitative real-time PCR showed an elevated Smad-2 gene expression in the hepatotoxicity group compared with that in the control group. In contrast, the treated groups demonstrated significantly lower Smad-2 mRNA levels compared with hepatotoxicity group (Figure 7B).

Effect of Tested Compounds on Gene Expression of Col1A1

As shown in Figure 7C, the expression level of Col1A1 in the hepatocytes of hepatotoxicity group was markedly increased when compared with that in the control group (P < 0.0001). The level of Col1A1 was decreased significantly compared with that in the hepatotoxicity group when the rats were treated with tested compounds and silymarin.

https://doi.org/10.2147/DDDT.S592956

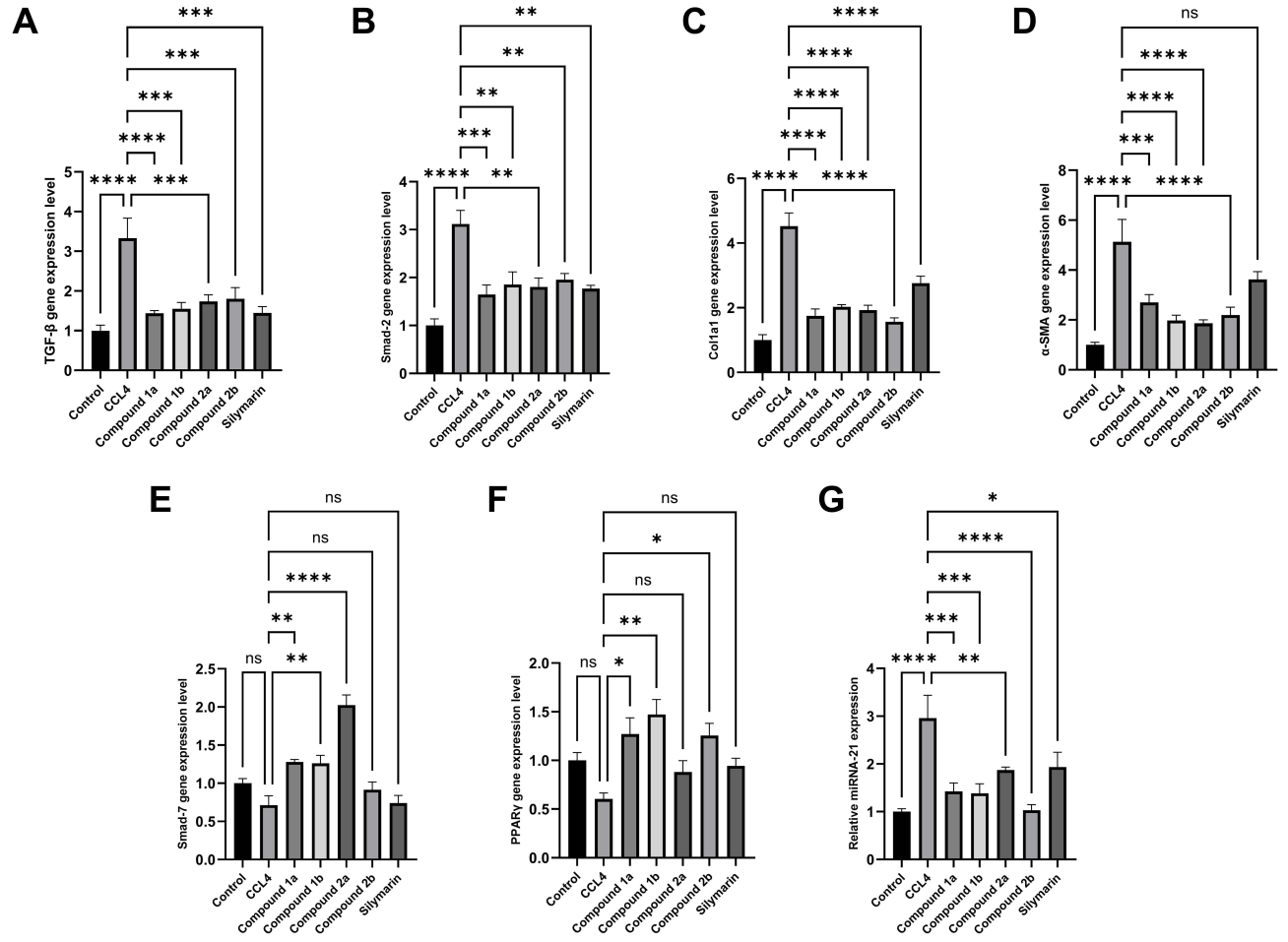

Figure 7 The effect of tested compounds on the TGF-β/miR-21/Smad7 signaling pathway at the gene expression level. Relative mRNA expression levels were determined by qPCR for (**A**) TGF-β, (**B**) Smad-2, (**C**) Col1A1, (**D**) α-SMA, (**E**) Smad-7, (**F**) PPARγ, and (**G**) miR-21. Data are presented as mean ± SEM. *p < 0.05, **p < 0.01, ***p < 0.001, ****p < 0.0001 compared with the hepatotoxicity group.

Effect of Tested Compounds on Gene Expression of α-SMA

Quantitative real-time PCR revealed that α-SMA gene expression was elevated in the hepatotoxicity group compared to the control group. In contrast, the groups treated with the tested compounds showed significantly lower α-SMA mRNA levels compared to the hepatotoxicity group, whereas the rats treated with silymarin exhibited a non-significant decrease in α-SMA mRNA levels compared to the hepatotoxicity group (Figure 7D).

Monitoring the Effects of the Tested Compounds on Other Regulatory Biomarkers of the TGF-β/Smad Pathway at the Gene Expression Level

Effect of Tested Compounds on Gene Expression of Smad-7

As illustrated in Figure 7E, the expression level of Smad-7 in the liver tissues of the group treated with compound 2a was significantly higher than that in the control group ($P < 0.0001$). Additionally, the levels of Smad-7 were significantly elevated in rats treated with compounds 1a, 1b, and 2a compared to the hepatotoxicity group. However, no significant increase in Smad-7 levels was observed in rats treated with compound 2b or silymarin.

Effect of Tested Compounds on Gene Expression of PPARγ

As depicted in Figure 7F, the mRNA levels of PPARγ were significantly elevated in the groups treated with compounds 1a, 1b and 2b compared to the hepatotoxicity group. However, treatment with compounds 2a and silymarin resulted in a non-significant increase in PPARγ mRNA levels compared to the hepatotoxicity group.

https://doi.org/10.2147/DDDT.S592956

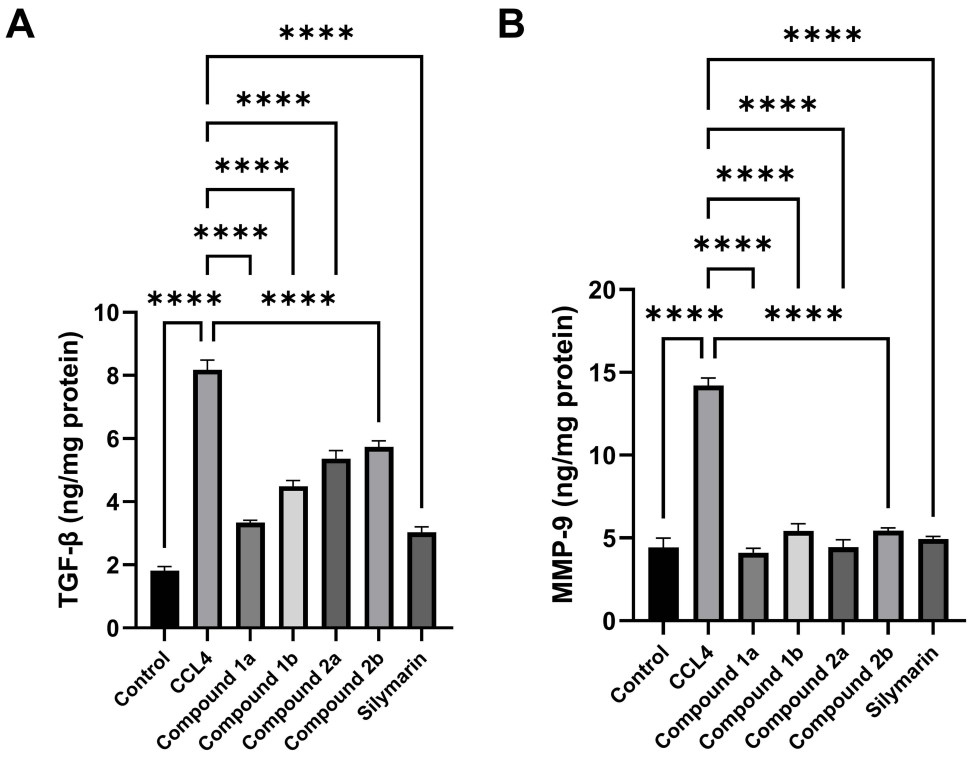

Figure 8 The effect of tested compounds on the protein expression of TGF-β and MMP-9. Protein levels of (**A**) TGF-β and (**B**) MMP-9 were measured using the ELISA technique. Data are presented as mean ± SEM. ****p < 0.0001 compared with the hepatotoxicity group.

Effect of Tested Compounds on Relative miRNA-21 Expression

Quantitative real-time PCR analysis revealed that the hepatotoxicity group exhibited a marked increase in relative miRNA-21 expression compared to the control group. Conversely, the groups treated with the tested compounds and silymarin showed a significant reduction in the relative miRNA-21 expression levels compared to the hepatotoxicity group (Figure 7G).

Monitoring the Effects of the Tested Compounds on the TGF-β and MMP-9 Biomarkers at Protein Level

The assessment of inflammatory and fibrotic cytokines, TGF-β, and one of the matrix metalloproteinases, MMP-9, both showed a significant increase within the hepatotoxicity group compared to control group, while both exhibit a significant decrease in the treated groups compared to hepatotoxicity group, as demonstrated in Figure 8A and B, respectively.

Molecular Modeling and Simulation

To rationalize the binding potential of the molecules to TGF-β, we conducted a docking experiment of these molecules on the crystal structure of TGF-β (PDB ID: 2wot) using FRED.[38] The results revealed that these compounds showed superior docking scores compared to co-crystal ligand, as shown in Table S1. in the SM.

Their postulated binding poses exhibited favorable interactions with the binding site residues of the TGF-β, as exhibited in Figures 9 and S1 in the SM. For instance, Compound **1a** (Figure 9A) exhibits H-bond interaction with LYS232 of the hinge region of the TGF-β.[39] Moreover, it is packed in the hydrophobic cleft formed by TYR249, LEU278 and VAL219 which can offer extra stability in the gatekeeper region.[40] Similarly, the phenyl group of **1b** is packed in the hydrophobic cleft formed by TYR249, LEU278 and VAL219 (Figure 9B). Compound **2a** exhibits a dual H-bond pattern with HIS283 and ASP281 of the hinge region while packed between LYS232, SER280 and VAL219, as shown in Figure 9C. This "bidentate" binding is a characteristic of powerful inhibitors indicating a high degree of complementarity with the TGF-β.[41] Compound **2b** forms H-bonds with HIS283, SER280, and ASP281, and hydrophobic

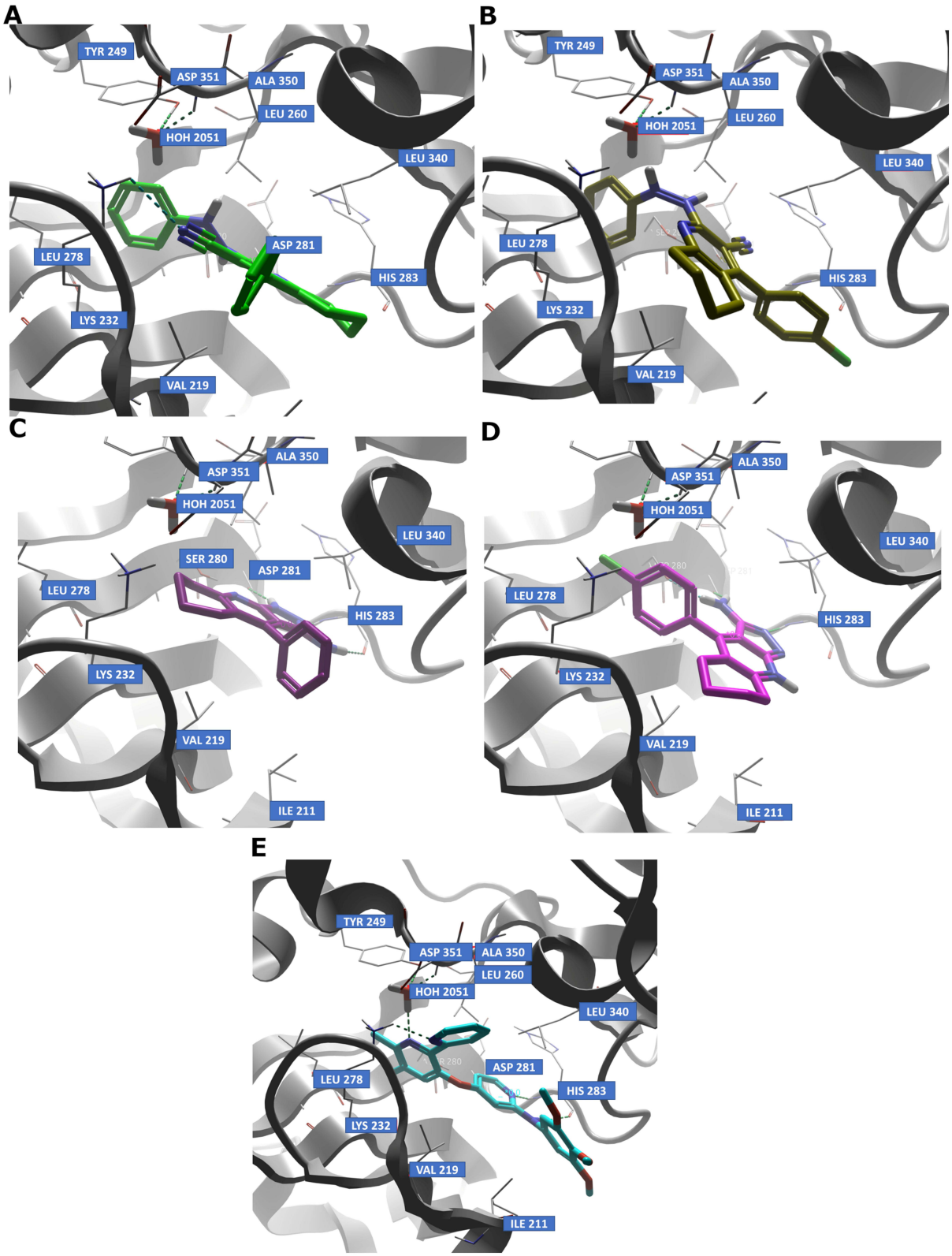

Figure 9 Docking poses of the compounds in the binding site of TGF-β. (**A**) Docking pose of **1a**. (**B**) Docking pose of **1b**. (**C**) Docking pose of 2a. (**D**) Docking pose of 2b. (**E**) Pose of the co-crystal ligand.

https://doi.org/10.2147/DDDT.S592956

interactions with VAL219 and ILE211, as seen in Figure 9D. All compounds displayed comparable hinge occupancy to the co-crystallized ligand (Figure 9E).

Molecular dynamics (MD) simulations lasting 100 ns were conducted on the TGF-β complexed with the ligand's docking pose in order to examine their time-stability in the binding sites. Additional MD run was carried out of the co-crystal structure of TGF-β as a reference for comparison.

MD analysis metrics, such as radius of gyration (Rg), and root mean square fluctuation (RMSF) are displayed and discussed in Figures S2 and S3 in the SM. Further details about the results and discussion of these metrics can be found in the SM.

The root mean square deviation (RMSD) metric is used to measure protein stability during the simulation period. The RMSD for the protein backbone and the ligands were measured. Generally, RMSD profiles of the four protein TGF-ligand complexes are comparable to the co-crystalized ligand protein complex, with RMSD values around 1.5 Å for the backbone (blue lines in Figure 10). This indicates that the protein structure remained stable throughout the simulations. For the ligand's RMSD (green lines in Figure 10), compounds **1a, 2a** and **2b** showed comparable stability and minor fluctuations in the binding site with RMSD values around 2 Å, 1 Å and 1 Å, as shown in Figure 10A, C and D, respectively. However, some fluctuations can be observed for **1b** between 20–60 ns simulation time, with RMSD values around 3–5 Å, as shown in Figure 10B. This may indicate some pose dynamics in the binding site for **1b**. The **1b** pose displayed hinge binding with some pi-pi stacking and hydrophobic interactions with TYR282. However, after 60 ns, the H-bonding interaction with HIS283 decays, while maintaining the initial pose's hydrophobic interactions with TYR249, LEU278 and VAL219, as seen in the ProLIF analysis in Figure S5 in the SM. This indicates its reasonable stability in the binding site of TGF-β. Overall, the ligands' RMSD behavior of **1a, 2a** and **2b** is comparable to the co-crystal ligand RMSD profile, as seen in Figure 10E.

Insights into the interactions profile of the ligand's pose during the simulation time are visualized and discussed in the SM and displayed in Figures S4–S7.

Discussion

The liver, one of the critical organs in our body, is essential for many functions as detoxifying chemicals, synthesizing proteins, metabolizing nutrients and drugs.[2] Liver fibrosis represents a reversible phase in the continuum of progression toward liver cirrhosis and hepatocellular carcinoma.[5] A significant contributor to liver failure is drug-induced hepatotoxicity, since liver is responsible for concentrating and metabolizing a majority of chemicals. CCl_4 is a commonly used chemical in research to study liver fibrosis and evaluate potential therapies. It induces liver damage through the formation of free radicals, causing inflammation and fibrosis.[17]

Previous research[18,23,24] has demonstrated that fused pyridine (tetrahydroquinoline) derivatives, designed based on the structure of tacrine, possess hepatoprotective properties. Further studies[14,27] on THQ derivatives have reinforced these findings, showing significant improvements in liver biomarkers and reductions in liver fibrosis.

This study evaluates the toxicity profile of four novel fused pyridine derivatives (tetrahydroquinolines and pyrazolo-tetrahydroquinoline) both in vivo using Sprague-Dawley rats and in vitro with HepG2 cells (a human hepatoma cell line widely used to study liver toxicity due to their ability to mimic hepatocyte function), alongside their hepatoprotective effects in a CCl_4-induced liver fibrosis rats model.

The in vitro cytotoxicity studies on the HepG2 cell line demonstrated that the four tested compounds exhibited a relatively safe hepatic profile, as increasing their concentrations did not significantly impact cell viability. In contrast, tacrine showed a dose-dependent decrease in cell viability.

A comprehensive in vivo toxicity assessment of the compounds was performed using both biochemical and histopathological analyses. Previous studies[42,43] have indicated that elevated transaminase levels (AST and ALT) are early markers of liver damage. Our study found that synthesized compounds not only showed a safe profile regarding hepatic biomarkers (ALT and AST) but compounds 2a and 2b notably reduced AST levels compared to the control group indicating the importance of the presence of a primary amino group for such activity regardless of the presence of the chloro-substitution of the 4-phenyl ring. In terms of lipid profile (serum cholesterol and triglycerides), no significant increase observed, demonstrating a safe profile.[44] The safety profile of the compounds was further confirmed through

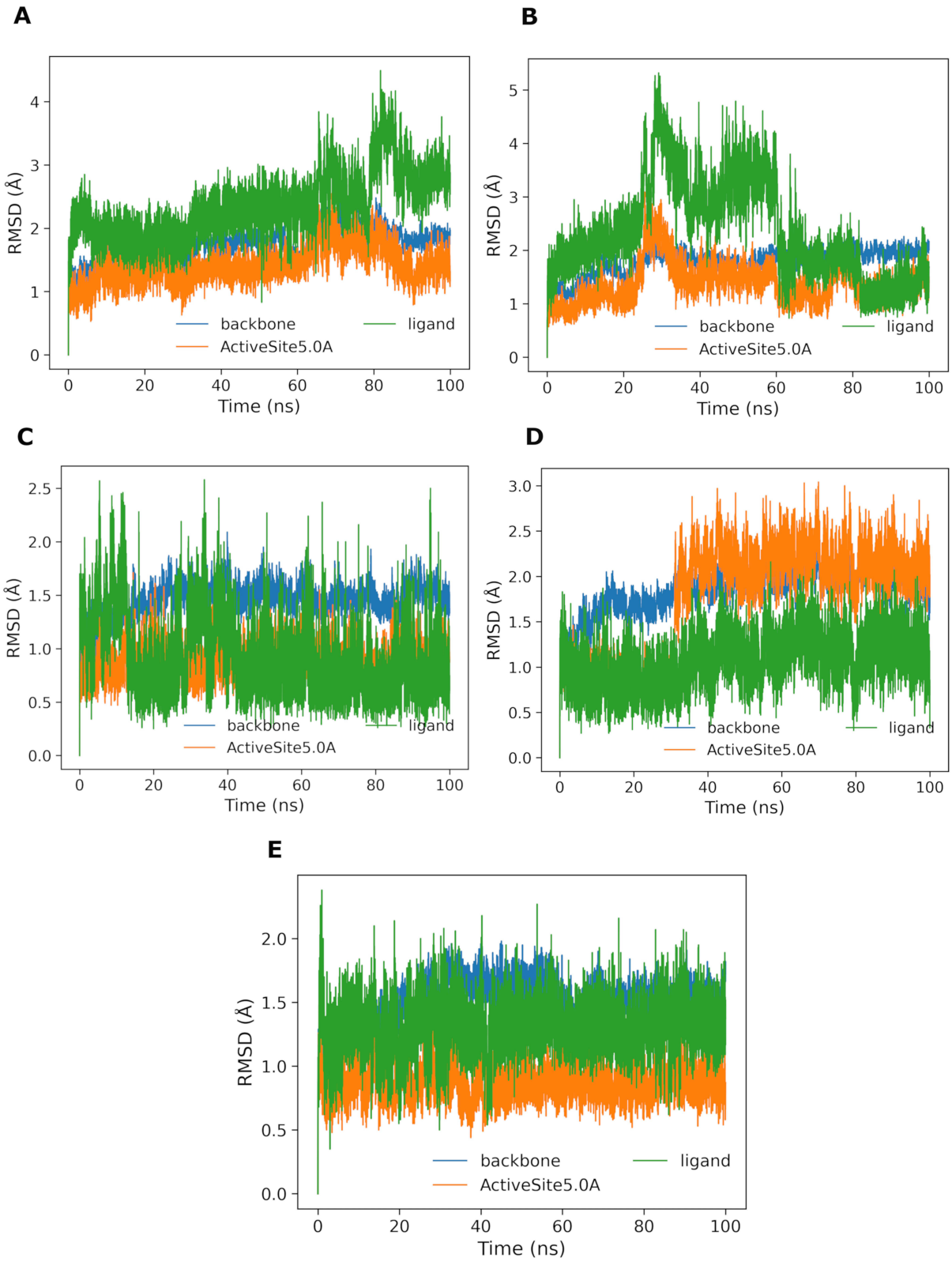

Figure 10 RMSD analysis of the TGF-β and ligand complex systems during the simulation time. (**A**) RMSD analysis of 1a and TGF-β complex system. (**B**) RMSD analysis of 1b and TGF-β complex system. (**C**) RMSD analysis of 2a and TGF-β complex system. (**D**) RMSD analysis of 2b and TGF-β complex system. (**E**) RMSD analysis of co-crystal ligand and TGF-β complex system. RMSD lines for protein backbone (blue line), for ligand heavy atoms (green line) and for active site residues (Orange line).

https://doi.org/10.2147/DDDT.S592956

histopathology using hematoxylin and eosin, as well as Masson's trichrome staining, which revealed normal liver architecture and healthy hepatocytes for all tested compounds. Based on these findings, the compounds can be considered not only safe but also potentially beneficial in certain aspects of hepatic toxicity studies.

Histopathological evaluation revealed that the control group maintained normal liver histology, with intact lobular structure, minimal fibrous tissue, and no inflammation. In contrast, the CCl_4-treated group exhibited severe liver disorganization, extensive fibrosis, and pronounced inflammation. Treatment with the fused pyridine derivatives led to substantial improvement in liver architecture, with reduced inflammation and fibrosis compared with hepatotoxicity group, which is evidenced by the decreased METAVIR activity and fibrosis scores. Among the treated groups, compound 2b provided the greatest protection, closely mirroring the effect of silymarin indicating the efficient protective effect of the primary amino group and the chloro-substitution. These results are supported by serological analyses, which demonstrated a significant reduction in liver enzymes (ALT, AST), ALP and total bilirubin in treated groups (IV–VII), further confirming the protective effects of the compounds against CCl_4-induced liver damage. All four compounds were as effective as silymarin (the reference drug) in significantly reducing elevated levels of transaminases (ALT and AST), ALP, and total bilirubin, bringing them close to the levels observed in the control group which suggests that minor changes in the structure has minor effect on the activity of these compounds indicating that the important pharmacophore for such activities is the 4-phenyltetrahydroquinoline moiety itself.

In this study, the role of various molecular pathways involved in liver fibrosis was explored, particularly focusing on the TGF-β/Smad, miR-21/Smad7, and PPARγ pathways, which play a crucial role in regulating extracellular matrix (ECM) deposition and liver fibrosis.[5,6,10,12,13]

TGF-β is a central mediator in liver fibrosis, playing a pivotal role in activating hepatic stellate cells (HSCs) and promoting extracellular matrix (ECM) deposition through its downstream Smad2/3 signaling pathway.[8] Elevated TGF-β levels are a hallmark of fibrogenesis and are associated with increased production of fibrotic markers such as collagen and α-SMA.[8–10] In our study, TGF-β mRNA and protein levels were significantly elevated in the CCl_4-induced liver fibrosis model, indicating active fibrogenesis. On the other hand, treatment with all four tested compounds and silymarin significantly reduced TGF-β levels, bringing them closer to control values, this again indicates the importance of the 4-phenyltetrahydroquinoline group with minor significance of substitution. The reduction in TGF-β levels suggests that the tested compounds effectively inhibited the primary driver of liver fibrosis. This suppression likely impacted downstream pathways, including Smad2/3 activation and the expression of fibrotic markers like α-SMA and collagen I, similar to silymarin, suggesting a potent anti-fibrotic effect by these compounds. This finding is consistent with studies by Sorour et al and Abdelgalil et al,[14,27] which reported that THQ reduces TGF-β levels in CCl_4-treated rats.

Smad2 and Smad3 are downstream mediators of TGF-β signaling, critical for transducing pro-fibrotic signals[8] Their phosphorylation and activation lead to the expression of fibrotic markers (α-SMA and Col1A1), making them a key target for antifibrotic therapies.[8,9] In the CCl_4-induced fibrosis model, Smad2 levels were significantly elevated, reflecting active TGF-β signaling. On the other hand, treatment with the four tested compounds and silymarin significantly reduced Smad2 levels. The suppression of Smad2 by the tested compounds, similar to silymarin, indicates a successful blockade of TGF-β/Smad signaling pathway. This inhibition likely leads to a reduction in downstream fibrotic markers, such as α-SMA and collagen I, effectively curbing ECM deposition and fibrosis progression. This reduction aligns with prior research indicating that suppressing these markers can effectively inhibit the progression of liver fibrosis.[5,6,13,45]

α-SMA is a key marker of activated myofibroblasts, which are responsible for excessive extracellular matrix (ECM) production in liver fibrosis.[5] Elevated α-SMA levels indicate hepatic stellate cell (HSC) activation, a critical step in fibrogenesis.[8,9] Our study found that α-SMA expression was significantly elevated in the hepatotoxicity group (group III), reflecting active fibrotic progression. However, treatment with the four tested compounds significantly reduced α-SMA levels which agree with the results of Sorour et al and Abdelgalil et al.[14,27] Compounds 1b, 2a and 2b bring α-SMA levels closer to control values, with compound 2a showing the strongest effect. This points out the importance of presence of an amino group regardless of whether it is primary or secondary, in addition to potential effect of the presence of a chloro-substitution at the 4-phenyl ring. The reduction in α-SMA levels, particularly with compounds 1b, 2a and 2b, suggests effective deactivation of myofibroblasts, helping to limit ECM production and overall fibrosis.[5,6] This

indicates that the compounds not only blocked TGF-β signaling but also prevented cellular activation central to fibrotic progression.

Col1A1 is a major component of the ECM. Increased Col1A1 level is a direct marker of fibrosis as excess collagen is deposited in liver tissue during fibrogenesis, leading to scar formation and tissue stiffness.[8,9] In this study, Col1A1 expression was significantly elevated in the hepatotoxicity group, indicating active fibrogenesis. On the other hand, the four treated groups as well as silymarin group effectively reduced Col1A1 levels. The reduction in Col1A1 expression, particularly with compounds 1a and 2b achieving near-control levels, suggests effective inhibition of ECM deposition and fibrosis.[5,6,12] Compounds 1a and 2b show significant reduction in Col1A1 level compared to silymarin clarifying the insignificance of the 4-chloro-substitution on this protein expression. This result correlates with the suppression of upstream regulators like TGF-β, Smad2, and α-SMA, indicating that the compounds successfully limited both signaling and fibrotic outcomes.

Smad7 is an inhibitory protein that regulates the TGF-β/Smad pathway by blocking Smad2/3 activation, thereby exerting anti-fibrotic effects.[8,12] Reduced levels of Smad7 lead to fibrogenic signaling, while higher levels help counteract TGF-β-induced fibrosis.[8] In the CCl_4 model, Smad7 levels were significantly reduced, reflecting diminished negative regulation of the TGF-β pathway. Treatment with compounds 1a, 1b, and 2a significantly elevated Smad7 levels, surpassing even those of the control group, suggesting the restoration of the inhibitory action. Such results eliminate the possibility of any significance of the chloro-substitution and clarify that its presence is not preferred in association with the presence of the primary amino group. The increase in Smad7, especially with compound 2a which is significant compared to both control and silymarin groups, indicates effective re-establishment of the regulatory balance in the TGF-β/Smad pathway.[8,12,13] This upregulation complements the reduction of TGF-β and Smad2, forming a comprehensive blockade against fibrotic progression.

miR-21 is a pro-fibrotic microRNA that enhances TGF-β signaling by inhibiting Smad7, thereby promoting fibrosis.[10] Elevated miR-21 levels are commonly observed in fibrotic tissues and contribute to the suppression of anti-fibrotic pathways.[13] In this study, miR-21 levels were significantly elevated in the hepatotoxicity group, sustaining fibrogenic signaling. Treatment with the four tested compounds significantly reduced miR-21 levels. On the other hand, silymarin did not reduce the level of miR-21 as done by tested compounds. The reduction in miR-21 levels, particularly with the tested compounds, relieved the suppression of Smad7, thus restoring its anti-fibrotic function.[9,10] This dual mechanism, lowering miR-21 and increasing Smad7, demonstrates the compounds' enhanced ability to block TGF-β/Smad signaling and inhibit fibrosis progression, which aligns with findings by Yang et al and Huang et al[10,13] who demonstrated that miR-21 inhibition reduced fibrosis.

PPARγ is a nuclear receptor that plays a key role in keeping HSCs in a quiescent state, thereby preventing fibrosis.[12] It is a key anti-fibrotic factor as it suppresses collagen production and reduces TGF-β expression.[46] Reduced PPARγ levels are associated with HSC activation, leading to increased ECM production and fibrotic progression.[46] In the CCl_4 model, PPARγ expression was significantly reduced, indicating active HSC transformation.[5] However, treatment with compounds 1a and 1b significantly increased PPARγ levels. These results further emphasize the significance of the secondary amino group present at the 2-position of the tetrahydroquinoline nucleus. The increase in PPARγ levels, especially with compound 1b which is significantly increased compared to both hepatotoxicity and silymarin groups, suggests a successful restoration of HSC quiescence, preventing their activation and reducing fibrosis.[12] This complements the reduction in α-SMA and collagen, highlighting the compounds' enhanced ability to inhibit fibrotic progression by maintaining PPARγ activity. These results are in line with earlier studies suggesting that PPARγ activation inhibits TGF-β signaling, thereby reducing collagen deposition and fibrosis.[5,12]

MMP-9 is involved in ECM degradation and remodeling.[8] Its elevated levels are often observed during fibrosis progression.[11] Excessive MMP-9 activity can exacerbate tissue damage and remodeling.[47] In the fibrosis model, MMP-9 levels were significantly elevated, reflecting active ECM turnover.[48] Treatment with all four compounds and silymarin reduced MMP-9 levels, with the compounds showing similar efficacy to silymarin in restoring MMP-9 to near-control levels. The reduction in MMP-9 by the tested compounds was comparable to silymarin, contributing to overall ECM stabilization. This effect, when combined with the reduction in collagen and α-SMA, suggests that the tested compounds

were equally effective as silymarin in preventing further matrix degradation and remodeling, aiding in the stabilization of liver tissue.[8,49]

Interestingly, among the proposed mechanisms of action of these compounds is the potential binding to TGF-β. The docking experiment and molecular dynamics simulations anticipate stable and high affinity binding of these compounds to the binding site of TGF-β.

These results emphasize the importance of the 4-phenyltetrahydroquinoline as the main pharmacophore for this pathway regardless of the substitutions present on the 2-, 3- and 4-positions, however, in most suggested proteins, the presence of 2 secondary amine groups and absence of a fused pyrazolo-ring were more preferable for activity except for their effect against AST enzyme.

Despite the comprehensive evaluation conducted in this study, certain limitations should be acknowledged. The mechanistic interpretation was primarily supported by gene expression analysis and selected protein measurements; therefore, further protein-level investigations, such as pSmad2/3, could provide additional confirmation of the signaling pathways involved. Future studies incorporating additional protein analyses would help to further elucidate the molecular mechanisms underlying the observed antifibrotic effects.

Conclusion

We can conclude that these four newly synthesized fused pyridine derivatives do not cause hepatotoxicity. On the other hand, they have hepatoprotective effects and mitigate liver damage by modulating the TGF-β/Smad signaling pathway, miR-21 expression, and PPARγ activity. This hepatoprotective effect is even more superior than silymarin, the reference drug, through a notable reduction in both α-SMA and Col1A1 and a significant increase in Smad7 and PPARγ levels.

Abbreviations

ECM, Extracellular matrix; HSCs, Hepatic stellate cells; TGF-β, Transforming growth factor-beta; SMAD, Suppressor of Mothers against Decapentaplegic; TIMPs, Tissue inhibitors of metalloproteinases; α-SMA, alpha-smooth muscle actin; MMPs, Matrix metalloproteinases; COL1A1, Collagen type I alpha 1; miR, Micro-Ribonucleic acid; PPAR-γ, Peroxisome proliferator-activated receptor-γ; SGOT, Serum glutamic-oxaloacetic transaminase; SGPT, Serum glutamate pyruvate transaminase; THQs, Tetrahydroquinoline; DMSO, Dimethyl sulfoxide; DMEM, Dulbecco's Modified Eagle Medium; FBS, Fetal bovine serum; CMC, Carboxymethyl cellulose.

Ethics Approval and Consent to Participate

The study has been approved by the Animal Care and Use Committee of the Faculty of Pharmacy, Alexandria University, Egypt (Approval Code. 06-2023-4–12-2-178).

Acknowledgments

The authors gratefully acknowledge the support of OpenEye Scientific Software Inc. for offering a free academic license.

Funding

This research received no funding.

Disclosure

The authors report no conflicts of interest in this work.

References

1. Ray G. Management of liver diseases: current perspectives. *World J Gastroenterol*. 2022;28(40):5818–5826. doi:10.3748/wjg.v28.i40.5818
2. Chiang JYL, Ferrell JM. Bile acid metabolism in liver pathobiology. *Gene Expr*. 2018;18(2):71–87. doi:10.3727/105221618X15156018385515
3. Di-Iacovo N, Pieroni S, Piobbico D, et al. Liver regeneration and immunity: a tale to tell. *Int J Mol Sci*. 2023;24(2):1176. doi:10.3390/ijms24021176
4. Zamani M, Alizadeh-Tabari S, Ajmera V, Singh S, Murad MH, Loomba R. Global prevalence of advanced liver fibrosis and cirrhosis in the general population: a systematic review and meta-analysis. *Clin Gastroenterol Hepatol*. 2025;23(7):1123–1134. doi:10.1016/j.cgh.2024.08.020

5. Yu Q, Cheng P, Wu J, Guo C. PPARgamma/NF-kappaB and TGF-beta1/Smad pathway are involved in the anti-fibrotic effects of levo-tetrahydropalmatine on liver fibrosis. *J Cell Mol Med*. 2021;25(3):1645–1660. doi:10.1111/jcmm.16267
6. Badr G, Sayed EA, Waly H, Hassan KA, Mahmoud MH, Selamoglu Z. The therapeutic mechanisms of propolis against CCl(4) -mediated liver injury by mediating apoptosis of activated hepatic stellate cells and improving the hepatic architecture through PI3K/AKT/mTOR, TGF-beta/Smad2, Bcl2/BAX/P53 and iNOS signaling pathways. *Cell Physiol Biochem*. 2019;53(2):301–322. doi:10.33594/000000140
7. Tsuchida T, Friedman SL. Mechanisms of hepatic stellate cell activation. *Nat Rev Gastroenterol Hepatol*. 2017;14(7):397–411. doi:10.1038/nrgastro.2017.38
8. Zhang Y, Hua L, Lin C, et al. Pien-Tze-Huang alleviates CCl(4)-induced liver fibrosis through the inhibition of HSC autophagy and the TGF-beta1/Smad2 pathway. *Front Pharmacol*. 2022;13:937484. doi:10.3389/fphar.2022.937484
9. Xu X, Hong P, Wang Z, Tang Z, Li K. MicroRNAs in transforming growth factor-beta signaling pathway associated with fibrosis involving different systems of the human body. *Front Mol Biosci*. 2021;8:707461. doi:10.3389/fmolb.2021.707461
10. Yang F, Luo L, Zhu ZD, et al. Chlorogenic acid inhibits liver fibrosis by blocking the miR-21-Regulated TGF-beta1/Smad7 signaling pathway in vitro and in vivo. *Front Pharmacol*. 2017;8:929. doi:10.3389/fphar.2017.00929
11. Duarte S, Baber J, Fujii T, Coito AJ. Matrix metalloproteinases in liver injury, repair and fibrosis. *Matrix Biol*. 2015;44–46:147–156. doi:10.1016/j.matbio.2015.01.004
12. Zhou D, Wang J, He LN, et al. Prolyl oligopeptidase attenuates hepatic stellate cell activation through induction of Smad7 and PPAR-gamma. *Exp Ther Med*. 2017;13(2):780–786. doi:10.3892/etm.2017.4033
13. Huang Q, Zhang X, Bai F, et al. Methyl helicterte ameliorates liver fibrosis by regulating miR-21-mediated ERK and TGF-beta1/Smads pathways. *Int Immunopharmacol*. 2019;66:41–51. doi:10.1016/j.intimp.2018.11.006
14. Abdelgalil MH, Elhammamy RH, Ragab HM, Sheta E, Wahid A. The hepatoprotective effect of 4-phenyltetrahydroquinolines on carbon tetrachloride induced hepatotoxicity in rats through autophagy inhibition. *Biol Res*. 2024;57(1):32. doi:10.1186/s40659-024-00510-4
15. Widowati W, Sabrina AHN, Sutendi AF, et al. Immune system and hepatic stellate cells' crosstalk in liver fibrosis: pathways and therapeutic potential. *J Immunol Res*. 2026;2026(1):2656395. doi:10.1155/jimr/2656395
16. Abdelgwad M, Ewaiss M, Sabry D, Khalifa WA, Altaib ZM, Alhelf M. Comparative study on effect of mesenchymal stem cells and endothelial progenitor cells on treatment of experimental CCL4-induced liver fibrosis. *Arch Physiol Biochem*. 2022;128(4):1071–1080. doi:10.1080/13813455.2020.1752256
17. Xiong H, Guo J. Targeting hepatic stellate cells for the prevention and treatment of liver cirrhosis and hepatocellular carcinoma: strategies and clinical translation. *Pharmaceuticals*. 2025;18(4):507. doi:10.3390/ph18040507
18. Ragab HM, Ashour HMA, Galal A, Ghoneim AI, Haidar HR. Synthesis and biological evaluation of some tacrine analogs: study of the effect of the chloro substituent on the acetylcholinesterase inhibitory activity. *Monatshefte Für Chemie*. 2016;147(3):539–552. doi:10.1007/s00706-015-1641-2
19. Laleu B, Rubiano K, Yeo T, et al. Exploring a tetrahydroquinoline antimalarial hit from the medicines for malaria pathogen box and identification of its mode of resistance as PfeEF2. *ChemMedChem*. 2022;17(22):e202200393. doi:10.1002/cmdc.202200393
20. Mendez-Luna D, Morelos-Garnica LA, Garcia-Vazquez JB, et al. Modifications on the tetrahydroquinoline scaffold targeting a phenylalanine cluster on Gper as antiproliferative compounds against renal, liver and pancreatic cancer cells. *Pharmaceuticals*. 2021;14(1):49. doi:10.3390/ph14010049
21. Park I, Lee W, Yoo Y, et al. Protective effect of tetrahydroquinolines from the edible insect *Allomyrina dichotoma* on LPS-induced vascular inflammatory responses. *Int J Mol Sci*. 2020;21(10). doi:10.3390/ijms21103406
22. Vesga LC, Kronenberger T, Tonduru AK, et al. Tetrahydroquinoline/4,5-dihydroisoxazole molecular hybrids as inhibitors of breast cancer resistance protein (BCRP/ABCG2). *ChemMedChem*. 2021;16(17):2686–2694. doi:10.1002/cmdc.202100188
23. Fayzrakhmanov D, Zykova S, Shurov S, et al. Pharmacoprophylaxis of liver diseases: creating a new hepatoprotector. *BIO Web Conf*. 2020;17. doi:10.1051/bioconf/20201700061
24. Ragab HM, Teleb M, Haidar HR, Gouda N. Chlorinated tacrine analogs: design, synthesis and biological evaluation of their anti-cholinesterase activity as potential treatment for Alzheimer's disease. *Bioorg Chem*. 2019;86:557–568. doi:10.1016/j.bioorg.2019.02.033
25. Mroueh M, Faour WH, Shebaby WN, Daher CF, Ibrahim TM, Ragab HM. Synthesis, biological evaluation and modeling of hybrids from tetrahydro-1H-pyrazolo[3,4-b]quinolines as dual cholinestrase and COX-2 inhibitors. *Bioorg Chem*. 2020;100:103895. doi:10.1016/j.bioorg.2020.103895
26. Shang XF, Morris-Natschke SL, Liu YQ, Li XH, Zhang JY, Lee KH. Biology of quinoline and quinazoline alkaloids. *Alkaloids Chem Biol*. 2022;88:1–47. doi:10.1016/bs.alkal.2021.08.002
27. Sorour AA, Aly RG, Ragab HM, Wahid A. Structure modification converts the hepatotoxic tacrine into novel hepatoprotective analogs. *ACS Omega*. 2024;9(2):2491–2503. doi:10.1021/acsomega.3c07126
28. Mosmann T. Rapid colorimetric assay for cellular growth and survival: application to proliferation and cytotoxicity assays. *J Immunol Methods*. 1983;65(1–2):55–63. doi:10.1016/0022-1759(83)90303-4
29. Zeashan H, Amresh G, Singh S, Rao CV. Hepatoprotective activity of Amaranthus spinosus in experimental animals. *Food Chem Toxicol*. 2008;46(11):3417–3421. doi:10.1016/j.fct.2008.08.013
30. Rao GM, Rao CV, Pushpangadan P, Shirwaikar A. Hepatoprotective effects of rubiadin, a major constituent of Rubia cordifolia Linn. *J Ethnopharmacol*. 2006;103(3):484–490. doi:10.1016/j.jep.2005.08.073
31. Goh CW, Aw CC, Lee JH, Chen CP, Browne ER. Pharmacokinetic and pharmacodynamic properties of cholinesterase inhibitors donepezil, tacrine, and galantamine in aged and young Lister hooded rats. *Drug Metab Dispos*. 2011;39(3):402–411. doi:10.1124/dmd.110.035964
32. Shomer NH, Allen-Worthington KH, Hickman DL, et al. Review of rodent euthanasia methods. *J Am Assoc Lab Anim Sci*. 2020;59(3):242–253. doi:10.30802/AALAS-JAALAS-19-000084
33. Bedossa P, Poynard T. An algorithm for the grading of activity in chronic hepatitis C. The METAVIR Cooperative Study Group. *Hepatology*. 1996;24(2):289–293. doi:10.1002/hep.510240201
34. Livak KJ, Schmittgen TD. Analysis of relative gene expression data using real-time quantitative PCR and the 2(-Delta Delta C(T)) Method. *Methods*. 2001;25(4):402–408. doi:10.1006/meth.2001.1262
35. Ivanova A, Mokshyna O, Polishchuk P. StreaMD: the toolkit for high-throughput molecular dynamics simulations. *J Cheminform*. 2024;16(1):123. doi:10.1186/s13321-024-00918-w

36. Abrahama MJ, Murtola T, Schulz R. High performance molecular simulations through multi-level parallelism from laptops to supercomputers. *SoftwareX*. 2015;1(2):6. doi:10.1016/j.softx.2015.06.001
37. Flare™, version 11. Cresset®, Litlington, Cambridgeshire, UK. https://cresset-group.com/software/flare/. Accessed March 30, 2026.
38. McGann M. FRED and HYBRID docking performance on standardized datasets. *J Comput Aided Mol Des*. 2012;26(8):897–906. doi:10.1007/s10822-012-9584-8
39. Laping NJ, Grygielko E, Mathur A, et al. Inhibition of transforming growth factor (TGF)-beta1-induced extracellular matrix with a novel inhibitor of the TGF-beta type I receptor kinase activity: SB-431542. *Mol Pharmacol*. 2002;62(1):58–64. doi:10.1124/mol.62.1.58
40. Ogunjimi AA, Zeqiraj E, Ceccarelli DF, Sicheri F, Wrana JL, David L. Structural basis for specificity of TGFβ family receptor small molecule inhibitors. *Cell Signal*. 2012;24(2):476–483. doi:10.1016/j.cellsig.2011.09.027
41. de Gouville AC, Boullay V, Krysa G, et al. Inhibition of TGF-beta signaling by an ALK5 inhibitor protects rats from dimethylnitrosamine-induced liver fibrosis. *Br J Pharmacol*. 2005;145(2):166–177. doi:10.1038/sj.bjp.0706172
42. Bénichou C. Criteria of drug-induced liver disorders. Report of an international consensus meeting. *J Hepatol*. 1990;11(2):272–276. doi:10.1016/0168-8278(90)90124-a
43. Devarbhavi H. An update on drug-induced liver injury. *J Clin Exp Hepatol*. 2012;2(3):247–259. doi:10.1016/j.jceh.2012.05.002
44. Ji Y, Gao Y, Chen H, Yin Y, Zhang W. Indole-3-acetic acid alleviates nonalcoholic fatty liver disease in mice via attenuation of hepatic lipogenesis, and oxidative and inflammatory stress. *Nutrients*. 2019;11(9):2062. doi:10.3390/nu11092062
45. Ganai AA, Husain M. Genistein attenuates D-GalN induced liver fibrosis/chronic liver damage in rats by blocking the TGF-beta/Smad signaling pathways. *Chem Biol Interact*. 2017;261:80–85. doi:10.1016/j.cbi.2016.11.022
46. Zardi EM, Navarini L, Sambataro G, et al. Hepatic PPARs: their role in liver physiology, fibrosis and treatment. *Curr Med Chem*. 2013;20(27):3370–3396. doi:10.2174/09298673113209990136
47. Hamada T, Fondevila C, Busuttil RW, Coito AJ. Metalloproteinase-9 deficiency protects against hepatic ischemia/reperfusion injury. *Hepatology*. 2008;47(1):186–198. doi:10.1002/hep.21922
48. Knittel T, Mehde M, Grundmann A, Saile B, Scharf JG, Ramadori G. Expression of matrix metalloproteinases and their inhibitors during hepatic tissue repair in the rat. *Histochem Cell Biol*. 2000;113(6):443–453. doi:10.1007/s004180000150
49. Yu Q, Stamenkovic I. Cell surface-localized matrix metalloproteinase-9 proteolytically activates TGF-beta and promotes tumor invasion and angiogenesis. *Genes Dev*. 2000;14(2):163–176. doi:10.1101/gad.14.2.163